Scripta Materialia 122 (2016) 50–53

Contents lists available at ScienceDirect

Scripta Materialia

journal homepage: www.elsevier.com/locate/scriptamat

Regular article

Martensitic transformation-induced hydrogen desorption characterized by utilizing cryogenic thermal desorption spectroscopy during cooling

Motomichi Koyama [a,*], Yuji Abe [b], Kei Saito [c], Eiji Akiyama [d], Kenichi Takai [e], Kaneaki Tsuzaki [a]

[a] Department of Mechanical Engineering, Faculty of Engineering, Kyushu University, Fukuoka 819-0395, Japan
[b] Department of Mechanical Engineering, Graduate School of Engineering, Kyushu University, Fukuoka 819-0395, Japan
[c] Graduate School of Science and Technology, Sophia University, Tokyo 102-8554, Japan
[d] Environment and Energy Materials Division, National Institute for Materials Science, Ibaraki 305-0047, Japan
[e] Department of Engineering and Applied Science, Sophia University, Tokyo 102-8554, Japan

ARTICLE INFO

Article history:
Received 7 March 2016
Received in revised form 6 May 2016
Accepted 6 May 2016
Available online xxxx

Keywords:
Martensitic phase transformation
Hydrogen desorption
Cryogenic thermal desorption spectroscopy
Austenitic steel
Hydrogen embrittlement

ABSTRACT

Hydrogen desorption associated with thermally induced α′ and ε martensitic transformations was characterized by cryogenic thermal desorption spectroscopy (C-TDS) during cooling. The utilization of a cooling process during C-TDS measurements revealed that the dominant factors in the hydrogen desorption related to the α′ and ε martensitic transformations were local changes in diffusivity and motions of transformation dislocations, respectively.

Investigations of hydrogen segregation, diffusion, and effusion processes have been conducted to clarify the underlying mechanisms of hydrogen embrittlement. The hydrogen motion and distribution properties depend on its solubility and diffusivity as well as trapping abilities of various phases and lattice defects in target materials. Moreover, when a material is deformed plastically, dislocation motions transport hydrogen atoms [1–3] to lattice defects, crystal/phase interfaces, or surfaces, leading to the hydrogen embrittlement [4].

In addition, the effects of martensitic transformations on the hydrogen motion/distribution must be considered when studying the hydrogen embrittlement mechanism of transformation-induced plasticity (TRIP) steels [5,6]. The martensitic transformation increases the lattice defect density and locally changes the solubility, diffusivity, and positions of hydrogen atoms. The changes in hydrogen atom positions mean their migrations due to motions of transformation dislocations. As mentioned above, these hydrogen-related changes significantly affect behavior of the hydrogen embrittlement. However, suitable techniques, which can be used to characterize the local effect of the martensitic transformation on the hydrogen-related parameters, have not been developed so far.

One of the relatively simple types of steel transformation is thermally induced martensitic transformation since its behavior and the related phenomena are not affected by various plasticity mechanisms that are accompanied by deformation-induced martensitic transformations. Therefore, the key to the first step in evaluating the effect of transformation is the characterization of the hydrogen desorption process resulting from the thermally induced martensitic transformation. Thermal desorption spectroscopy (TDS) is one of the well-known, sensitive methods of detecting diffusible hydrogen species [7–9], which play an important role on the hydrogen embrittlement [10,11]. In fact, extra hydrogen desorption due to reverse transformation from ε-martensite to austenite has been recently detected by TDS [12]. However, the real objective is the hydrogen desorption caused by the forward transformation, since the TRIP effect originates from the forward martensitic transformation. To investigate hydrogen desorption due to the thermally induced martensitic transformation, the related TDS measurements must be performed during cooling to a cryogenic temperature, which is below the starting temperature for martensitic transformation (M_s). In recent years, a cryogenic TDS technique (C-TDS) has been developed to measure hydrogen desorption rates at cryogenic temperatures [12,13]. Utilization of the C-TDS can be a new tool for studying hydrogen desorption due to the thermally induced martensitic transformation. More specifically, the C-TDS profiles obtained during cooling would contain important information pertinent to the resulting cooling-induced phenomena such as martensitic transformations. However, effective utilization of the cooling process for C-TDS has never been attempted. Hence, the purpose of this work was to explore the correlation between the martensitic transformation behavior and the cooling-induced hydrogen desorption process by using the C-TDS technique.

* Corresponding author.
E-mail address: koyama@mech.kyushu-u.ac.jp (M. Koyama).

http://dx.doi.org/10.1016/j.scriptamat.2016.05.012
1359-6462/

Fe-31Ni and Fe-15Mn-10Cr-8Ni (mass%) austenitic alloys were prepared by vacuum induction melting. The alloys were selected by considering the following four factors. (1) The initial constituent phase should be fully austenitic. (2) The M_s temperatures for the α′ martensitic transformation in the Fe-31Ni alloy [14] and the ε martensitic transformation in the Fe-15Mn-10Cr-8Ni alloy [15] must lie between 100 K and the ambient temperature. (3) The estimated Néel temperature of the Fe-15Mn-10Cr-8Ni alloy should be around or lower than its M_s temperature [15,16] to avoid the effect produced by magnetic transition, which counteracts the ε-martensitic transformation process [17]. (4) Mobile interstitial elements should not be included to simplify the motion of interstitial hydrogen atoms at ambient temperature. The obtained steel ingots were forged and rolled at 1273 K. Subsequently, the steels were solution-treated at 1273 K for 1 h followed by water quenching to suppress uncontrolled precipitation and segregation. In addition, commercial tempered martensitic steel (Fe-0.31C-1.64Si-0.75Mn-0.009P-0.0004S), which is stable at low-temperature conditions, has been utilized as a reference material to characterize the standard hydrogen desorption behavior during cooling. The steel was first subjected to heat treatment at 1296 K, then water-quenched, and finally tempered at 743 K. All samples were cut by spark machining, and their thicknesses were reduced by mechanical grinding and subsequent electro-chemical polishing.

X-ray diffraction (XRD) measurements were conducted by using Co K_α at a voltage of 40 kV and scanning rate of 0.05°/s to characterize the constituent phase. The specimens utilized for the XRD measurements were 15 mm wide, 15 mm long, and 0.2 mm thick. M_s temperatures were determined by a differential scanning calorimeter (DSC) operated at a cooling rate of 20 K min^{-1} using 0.2 mm thick specimens with diameters of 3 mm.

To perform C-TDS measurements, Fe-31Ni and Fe-15Mn-10Cr-8Ni alloy specimens with widths of 8 mm, lengths of 8 mm, and thicknesses of 0.2 mm were hydrogen-charged at a current density of 100 A m^{-2} at 303 K for 72 h in a 0.1 N NaOH aqueous solution containing 5 g L^{-1} of NH_4SCN. A platinum wire was used as a counter electrode for the hydrogen charging process. Hydrogen atoms were introduced into a tempered martensitic steel specimen with a thickness of 0.2 mm and a diameter of 7.2 mm by its immersion into a 20 mass% NH_4SCN aqueous solution at 303 K for 24 h. The specimens were transferred to a chamber of the C-TDS within 5 min after the hydrogen charging. Then, it takes 15 min to evacuate the TDS chamber until 2×10^{-7} Pa before the C-TDS was started. The C-TDS was performed between 100 K and 450 K using a quadrupole mass spectrometer. First, the specimens were cooled from ambient temperature to 100 K at a cooling rate of 60 K h^{-1} to investigate the cooling-induced hydrogen desorption. After that, they were heated from 100 K to 450 K at a heating rate of 180 K h^{-1} to characterize the difference between the corresponding hydrogen desorption behaviors during the cooling and heating stages. The heating rate was chosen to be higher than the cooling rate to save experiment duration. The increase in heating rate shifts a peak position to a higher temperature side. Depth of the hydrogen-affected zone from the specimen surfaces of the austenitic alloys is estimated to be an order of 10 μm, accordingly to $(Dt)^{-1/2}$ criterion where D is assumed to be 10^{-16} m^2/s [18]. Namely, the hydrogen-charging time is insufficient for obtaining homogeneous hydrogen distribution. Therefore, the hydrogen desorption rate is shown as that per surface area i.e., μmol/cm^2 s [19].

Fig. 1 shows the XRD profiles of the Fe-31Ni and Fe-15Mn-10Cr-8Ni alloys before and after cooling to 77 K, which exhibit the α′ and ε martensitic transformations during cooling. Volume fractions of the retained austenite in the cooled Fe-31Ni and Fe-15Mn-10Cr-8Ni alloys were calculated to be 5% and 57%, respectively. Moreover, the hydrogen desorption profile for the tempered steel presented in Fig. 2 reveals a monotonic decrease in the hydrogen desorption rate with temperature without a characteristic peak. This fact indicates that extra hydrogen desorption does not occur when cooling does not induce martensitic

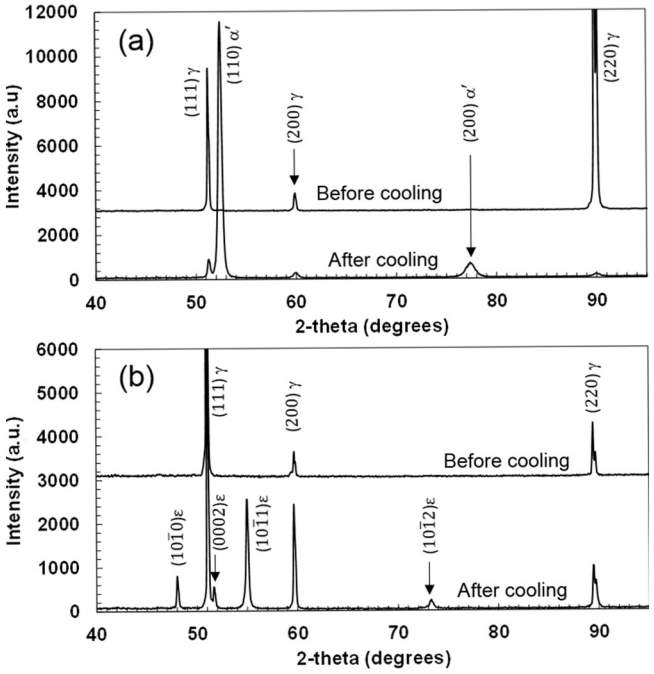

Fig. 1. XRD profiles of the two austenitic alloys before and after cooling to 77 K ub the (a) Fe-31Ni and (b) Fe-15Mn-8Ni-10Cr alloys.

transformation. In addition, the hydrogen desorption behavior of the heating process showed almost the same behavior of the cooling process at cryogenic temperatures below 250 K. Starting with the next paragraph, we will describe the effects of the α′ and ε martensitic transformations on the C-TDS profiles obtained during the cooling stage.

Fig. 3a demonstrates the effect of the α′ martensitic transformation in the Fe-31Ni alloy. Fig. 3b depicts a magnified graph of the low-temperature region in Fig. 3a where the characteristic peak appeared during cooling. As shown in Fig. 3c, the onset of the peak corresponded to the M_s temperature for the α′ martensitic transformation; the peak ended after the martensitic transformation was complete. The following two factors that affect the hydrogen desorption associated with the martensitic transformation should be considered: (1) local changes in hydrogen diffusivity (the diffusivities of α′-martensite and austenite at ambient temperature are of the orders of 10^{-11} [20] and 10^{-16} m^2/s

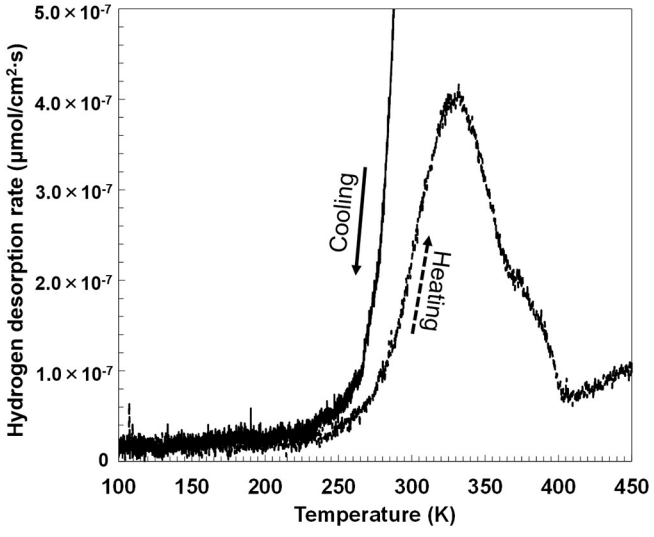

Fig. 2. Hydrogen desorption profile including the cooling stage in the tempered martensitic steel.

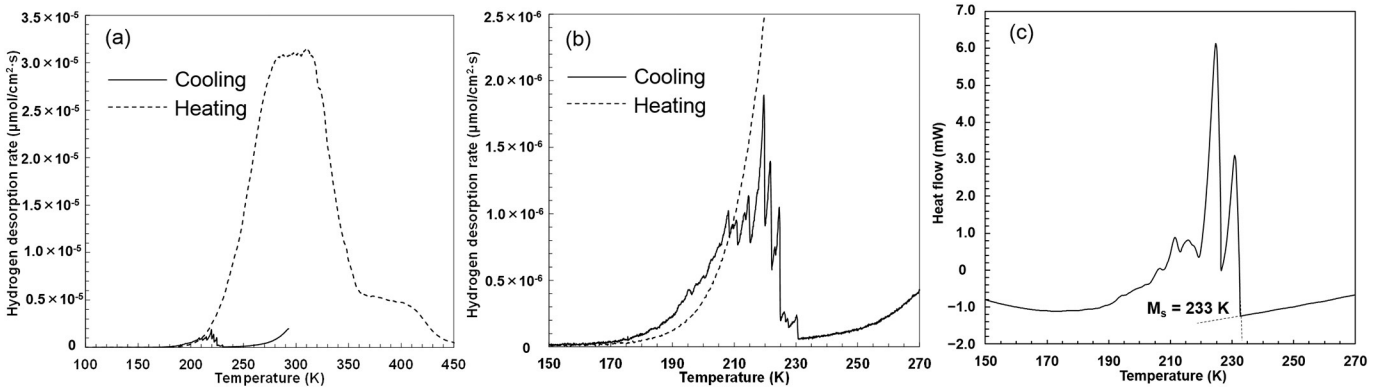

Fig. 3. (a) Cooling-induced hydrogen desorption in the Fe-31 alloy. (b) A magnified low-temperature region of the hydrogen desorption profile depicted in (a). The cooling and heating rates were 60 and 180 K h^{-1}, respectively. (c) A DSC spectrum for the Fe-31Ni alloy. The A_s temperature was measured to be 628 K.

[18], respectively) and (2) motions of hydrogen-decorated transformation dislocations. The density of lattice defects (such as transformation twins and dislocations) are usually affected by transformations, and the martensitic transformation increases the lattice defect density. The increase in lattice defect density rather suppresses hydrogen desorption through hydrogen trapping. In this work, we have focused on relative shape differences for the TDS profiles obtained during the cooling and heating stages. Since the motion of transformation dislocations affect the hydrogen desorption behavior only during cooling (when the temperature range is below the starting temperature for the reverse transformation), the TDS profiles obtained during heating exhibit completely different features from those obtained during cooling. In contrast, local changes in hydrogen diffusivity similarly affect both the cooling and heating processes below the finish temperature of the forward martensitic transformation. In the Fe-31Ni alloy, the α′ martensitic transformation is almost finished at around 200–210 K as shown in Fig. 3c. A similar trend is demonstrated in Fig. 3b, which displays the hydrogen desorption rate as a function of temperature during the heating and cooling processes. This fact indicates that the local changes in diffusivity are the dominant factor, resulting in the extra hydrogen desorption during cooling (although the effect of the transformation dislocation motions may slightly affect the related desorption behavior).

The TDS profile for the Fe-15Mn-10Cr-8Ni alloy is shown in Fig. 4a. The magnified region of the graph depicted in Fig. 4b exhibits a small peak during the cooling stage. The onset temperature of the peak (around 240 K) corresponds to the M_s temperature for the ε martensitic transformation (see Fig. 4c), which indicates that the peak obtained by the TDS measurement during cooling originates from the thermally induced ε martensitic transformation. Similar to the α′ martensitic transformation, the two factors associated with the diffusivity changes and transformation dislocation motions should be considered. Discussing changes in hydrogen diffusivity may be problematic for this particular case because the diffusion of hydrogen species in ε-martensite has never been studied. However, we have observed similar extra hydrogen desorption even when the ε → γ reverse transformation occurs [12] (in the present case, the hydrogen desorption accompanied with the reverse transformation with the A_s temperature of 336 K seems to be included in the large peak existing just above room temperature shown in Fig. 4a). If relatively high hydrogen diffusivity in ε-martensite is assumed (which may be a critical factor, resulting in a peak appearance during cooling), the reverse transformation must decrease the hydrogen desorption rate. In other words, the effect of diffusivity changes can be ruled out for the reason of the hydrogen desorption associated with the ε martensitic transformation. Moreover, ε-martensite is characterized by a close-packed structure, which is similar to that of austenite, implying that diffusivities of ε-martensite and austenite are also be similar. Since both the forward and reverse transformations produced the extra hydrogen desorption, it can be concluded that the cooling-induced desorption of hydrogen results from the motions of the transformation dislocations.

In conclusion, the utilization of the cooling process of C-TDS helped to partially clarify the underlying relationship between the hydrogen desorption and martensitic transformations. As a result, both the α′ and ε martensitic transformations induced the hydrogen desorption. The dominant factor causing the hydrogen desorption during the α′ martensitic transformation corresponded to the local changes in hydrogen diffusivity, while the hydrogen desorption during the ε martensitic transformation resulted from the motions of hydrogen-decorated transformation dislocations. The obtained results can be utilized to study a dynamic effect of the hydrogen distribution on the hydrogen embrittlement susceptibility of the TRIP steels. For instance, the hydrogen distribution in the TRIP steel is speculated to change during plastic

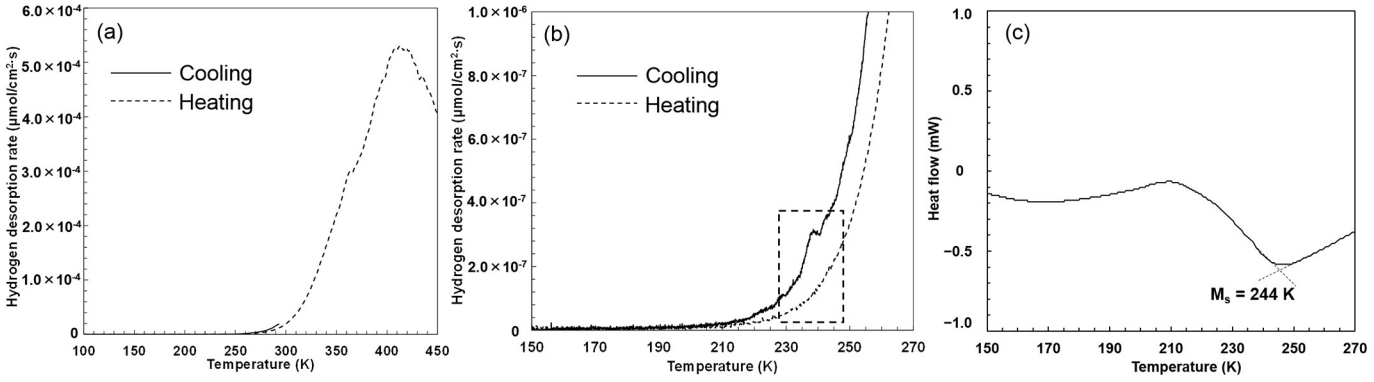

Fig. 4. (a) A Hydrogen desorption profile for the Fe-15Mn-10Cr-8Ni alloy, which includes the cooling stage. (b) A magnified low-temperature region of the hydrogen desorption profile depicted in (a). The cooling and heating rates were 60 and 180 K h^{-1} respectively. (c) A DSC spectrum for the Fe-31Ni alloy. The A, temperature was measured to be 336 K.

deformation by a simultaneous effect of slip dislocation motion and phase transformation, which complicates effects of the TRIP phenomenon on hydrogen embrittlement. The present study revealed the hydrogen desorption behavior when the martensitic transformation occurs without slip deformation.

Acknowledgement

The samples for this work were produced at the Materials Manufacturing and Engineering Station of National Institute for Materials Science (NIMS). The research project was supported by the Japan Science and Technology Agency (JST) (grant number: 20100113) under Industry-Academia Collaborative R&D Program "Heterogeneous Structure Control: Towards Innovative Development of Metallic Structural Materials".

References

[1] J. Tien, A.W. Thompson, I.M. Bernstein, R.J. Richards, Metall. Trans. A 7 (1976) 821–829.
[2] G.S. Frankel, R.M. Latanision, Metall. Trans. A 17 (1986) 869–875.
[3] H. Shoda, H. Suzuki, K. Takai, Y. Hagihara, ISIJ Int. 50 (2010) 115–123.
[4] M. Koyama, E. Akiyama, K. Tsuzaki, D. Raabe, Acta Mater. 61 (2013) 4607–4618.
[5] J.H. Ryu, Y.S. Chun, C.S. Lee, H.K.D.H. Bhadeshia, D.W. Suh, Acta Mater. 60 (2012) 4085–4092.
[6] M. Koyama, C.C. Tasan, T. Nagashima, E. Akiyama, D. Raabe, K. Tsuzaki, Philos. Mag. Lett. 96 (2016) 9–18.
[7] J.-Y. Lee, S.M. Lee, Surf. Coat. Technol. 28 (1986) 301–314.
[8] D. Pérez Escobar, T. Depover, L. Duprez, K. Verbeken, M. Verhaege, Acta Mater. 60 (2012) 2593–2605.
[9] M. Koyama, A. Bashir, M. Rohwerder, S.V. Merzlikin, E. Akiyama, K. Tsuzaki, D. Raabe, J. Electrochem. Soc. 162 (2015) C638–C647.
[10] K. Takai, R. Watanuki, ISIJ Int. 43 (2003) 520–526.
[11] M. Wang, E. Akiyama, K. Tsuzaki, Scr. Mater. 52 (2005) 403–408.
[12] M. Koyama, K. Tsuzaki, ISIJ Int. 55 (2015) 2269–2271.
[13] N. Abe, H. Suzuki, K. Takai, N. Ishikawa, H. Sueyoshi, Materials Science and Technology Conference and Exhibition 2011, MS and T'11, 2011 1277–1284.
[14] A. Shibata, S. Morito, T. Furuhara, T. Maki, Acta Mater. 57 (2009) 483–492.
[15] T. Sawaguchi, I. Nikulin, K. Ogawa, K. Sekido, S. Takamori, T. Maruyama, Y. Chiba, A. Kushibe, Y. Inoue, K. Tsuzaki, Scr. Mater. 99 (2015) 49–52.
[16] S. Curtze, V.T. Kuokkala, A. Oikari, J. Talonen, H. Hänninen, Acta Mater. 59 (2011) 1068–1076.
[17] A. Sato, E. Chishima, Y. Yamaji, T. Mori, Acta Metall. 32 (1984) 539–547.
[18] P. Tsong-Pyng, C.J. Altstetter, Acta Metall. 34 (1986) 1771–1781.
[19] M. Koyama, E. Akiyama, T. Sawaguchi, K. Ogawa, I.V. Kireeva, Y.I. Chumlyakov, K. Tsuzaki, Corros. Sci. 75 (2013) 345–353.
[20] W.C. Luu, J.K. Wu, Corros. Sci. 38 (1996) 239–245.